Reversals of the magnetic field generated by a turbulent flow

S. Fauve, E. Dormy, C. Gissinger and F. Pétrélis

Ecole Normale Supérieure, LPS - CNRS, 24 Rue Lhomond, 75005 Paris, France.
fauve@lps.ens.fr

When averaged on a few thousands years, the Earth's magnetic field can be roughly described as the one of an axial dipole. As shown by paleomagnetic records, it has frequently reversed its polarity on geological time scales. Field reversals have also been reported in several numerical simulations of the geodynamo and more recently, in a laboratory experiment involving a von Karman swirling flow of liquid sodium (VKS). We first recall some of the main experimental results and understand them using phenomenological models and numerical simulations. In particular, we show that all the regimes of the magnetic field observed in the experiments reported so far, can be understood in the framework of low dimensional dynamical system theory: two modes of the magnetic field, with dipolar (respectively quadrupolar) symmetry, can be generated by the turbulent flow of liquid sodium, and their interaction can lead to the observed dynamics (oscillations, random reversals, symmetric or asymmetric bursts). Turbulent fluctuations alone do not drive these dynamical regimes that only occur when a symmetry of the flow is broken. Although the flow in the Earth's core strongly differs from the one of the VKS experiment, a similar model but based on a different broken symmetry, can be used. It explains several features observed in paleomagnetic recordings of the Earth's magnetic field reversals.

1 A dynamo generated by a von Karman swirling flow

The generation of magnetic field by the flow of an electrically conducting fluid, i.e., the dynamo effect, is an instability that has been mostly studied to understand the magnetic fields of planets and stars [1]. Flows in the interiors of planets or stars have huge kinetic Reynolds numbers, $Re = VL/\nu$, where V is the typical velocity, L is its integral length scale and ν is the kinematic viscosity. For instance, $Re \sim 10^9$ in the Earth's liquid core or $Re \sim 10^{15}$ in the convective zone of the Sun. The main control parameter for dynamo action is the magnetic Reynolds number, $R_m = \mu_0 \sigma V L$. It relates transport

B. Eckhardt (ed.), *Advances in Turbulence XII*, Springer Proceedings in Physics 132,
DOI 10.1007/978-3-642-03085-7_193,

and stretching of the magnetic field by the flow to Ohmic diffusion (σ is the electrical conductivity and μ_0 is the magnetic permeability of vacuum). $P_m = R_m/Re = \mu_0\sigma\nu$ is the magnetic Prandtl number of the fluid. For planetary or stellar interiors, $P_m < 10^{-6}$. For liquid metals used in laboratory experiments, its maximum value is obtained with liquid sodium $P_m \sim 10^{-5}$. A necessary condition for dynamo action being R_m large enough in order to overcome Ohmic dissipation (in the range $10 - 100$ for many dynamos), the dynamo threshold can be reached only when the flow is strongly turbulent (Re of order 10^6 or larger). This provides both the difficulty and the interest of the problem. An instability that develops on a fully turbulent flow involves several open questions: Do turbulent fluctuations inhibit or enhance the growth rate of the magnetic field? What is the magnetic energy density that can by generated by a turbulent flow [2]? At which spatial scales is it maximum [3]? The first successful experiments on fluid dynamos involved flows with a geometrical confinement to aim at the suppression of large scale turbulence [4]. In contrast, the motivation for the von Karman geometry was to study the generation of a magnetic field by a strongly turbulent flow. The flow of liquid sodium is driven in a cylinder by two counter-rotating disks fitted with eight blades (see figure 1a). $Re \sim 5\,10^6$, thus $R_m \sim 50$ can be reached, and turbulent fluctuations are comparable to the mean flow (time averaged). The motivation for choosing this flow resulted from its strong differential rotation and the absence of mirror symmetry (in the counter-rotating case). In addition, this flow was known to generate tornado-like vorticity filaments [5] involving large velocity increments as displayed by pressure measurements [6]. All these features were known to favor dynamo action [7]. The generation of magnetic field by the VKS flow has been widely reported [8, 9, 10, 11] and we refer to these publications for a description of the experimental results. Our purpose here is to present various models and numerical simulations that provide an explanation for several experimental observations.

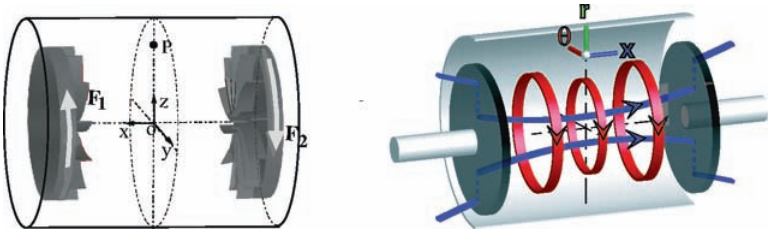

Fig. 1. a) Sketch of the von Karman swirling flow geometry. b) Sketch of the mean magnetic field generated for exact counter-rotation of the propellers, $F_1 = F_2$.

2 Geometry of the mean magnetic field: equatorial versus axial dipoles

Several early attempts to predict the magnetic field generated by the VKS flow and to understand the underlying mechanisms were presented in [12]. An equatorial dipole was found (as the one displayed in figure 2 (left) whereas the magnetic field observed in the experiment involved a strong axial dipolar component (see figure 1, right). These calculations were based on the mean flow of the VKS experiment. This one being axisymmetric, the generated magnetic field should break axisymmetry according to Cowling theorem [7] and this is achieved by an equatorial dipole. The experimental observation of an axial dipole thus shows that non axisymmetric velocity fluctuations play an important role in the VKS dynamo that is not generated by the mean flow alone. It has been proposed that the vortical flow radially ejected by the blades of the rotating impellers generate an axial mean field from an $\alpha-\omega$ mechanism [13]. This mechanism has been qualitatively illustrated using the mean field induction equation [14]. It has been checked using the direct numerical simulation displayed in figure 2 (right) [15]. It has been also shown by direct simulations of a flow generated by two propellers in a spherical domain, that an axial dipole is generated as soon as turbulent fluctuations are large enough [16].

Fig. 2. Numerical simulations of the magnetic field at dynamo threshold: left: an equatorial dipole is obtained when only the mean flow is taken into account. Right: an axial dipole is generated when non axisymmetric components in the form of vortices generated by the blades are included in the velocity field.

Thus, the VKS dynamo is not generated by the mean flow alone in contrast to Karlsruhe and Riga experiments, and non-axisymmetric fluctuations play an essential role in the dynamo process. Note also that it has been observed so far only when impellers made of soft iron have been used. It has been shown

that magnetic boundary conditions corresponding to the high permeability limit significantly decrease the dynamo threshold [17]. However, other mechanisms due to the iron disks can be also put forward (see for instance [13]).

3 Broken symmetries and dynamics of the large scale magnetic field

The most striking feature of the VKS experiment is that time dependent magnetic fields are generated only when the impellers rotate at different frequencies [9]. We will show that this can be related to the additional invariance under $\mathcal{R}_\pi$ when $F_1 = F_2$ (rotation of an angle π along any axis in the mid-plane). We indeed expect that in that case, the modes involved in the dynamics are either symmetric or antisymmetric. Such modes are displayed in figure 3. A dipole is changed to its opposite by $\mathcal{R}_\pi$, whereas a quadrupole is unchanged. More generally, we name "dipole" (respectively "quadrupole"), modes with dipolar (respectively quadrupolar) symmetry even though they might involve a more complex spatial structure.

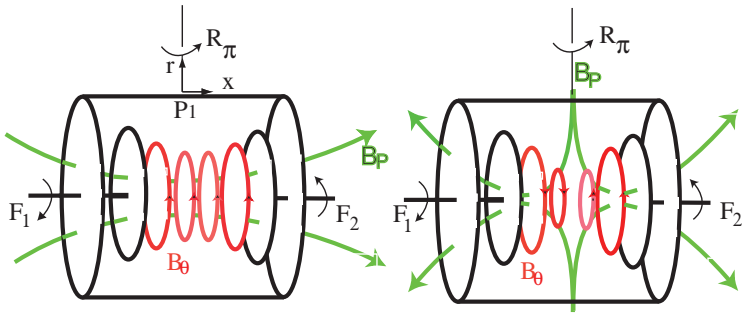

Fig. 3. Possible eigenmodes of the VKS experiment. The two disks counter-rotate with frequency F_1 and F_2. Left: magnetic dipolar mode. Right: magnetic quadrupolar mode. Poloidal, B_P, and toroidal, B_θ, components are sketched.

We assume that the magnetic field is the sum of a dipolar component with an amplitude D and a quadrupolar one, Q. We define $A = D + i\,Q$ and we assume that an expansion in power of A and its complex conjugate $\bar{A}$ is pertinent close to threshold in order to obtain an evolution equation for both modes. Taking into account the invariance $\mathbf{B} \to -\mathbf{B}$, *i.e.* $A \to -A$, we obtain

$$\dot{A} = \mu A + \nu \bar{A} + \beta_1 A^3 + \beta_2 A^2 \bar{A} + \beta_3 A \bar{A}^2 + \beta_4 \bar{A}^3 \,, \tag{1}$$

where we limit the expansion to the lowest order nonlinearities. In the general case, the coefficients are complex and depend on the experimental parameters.

Symmetry of the experiment with respect to $\mathcal{R}_\pi$ when the disks exactly counter-rotate, amounts to constraints on the coefficients. Applying this transformation to the magnetic modes, changes D into $-D$ and Q into Q, thus $A \to -\bar{A}$. We conclude that, in the case of exact counter-rotation, all the coefficients are real. When the frequency difference $f = F_1 - F_2$ is increased from zero, we obtain that the real parts of the coefficients are even and the imaginary parts are odd functions of f. When the coefficients are real, the growth rate of the dipolar component is $\mu_r + \nu_r$ and that of the quadrupolar component is $\mu_r - \nu_r$. The dipole being observed for exact counter-rotation implies that $\nu_r > 0$ for $f = 0$. By increasing f, we expect that ν_r changes sign and favors the quadrupolar mode according to the experimental results (see figure 3 in [10]). We will explain in the next section how modifying the parameters of (1) leads to bifurcation to time dependent solutions.

4 A mechanism for oscillations and reversals

As shown in [18], the planar system (1) explains the dynamical regimes observed so far in the VKS experiment [10]. It is invariant under the transformation $\mathbf{B} \to -\mathbf{B}$. Thus, in the case of counter-rotating impellers, $F_1 = F_2$, it has two stable dipolar solutions $\pm D$ and two unstable quadrupolar solutions $\pm Q$. When the frequency difference f is increased, these solutions become more and more mixed due to the increase of the strength of the coupling terms between dipolar and quadrupolar modes. Dipolar (respectively quadrupolar) solutions get a quadrupolar (respectively dipolar) component and give rise to the stable solutions $\pm B_s$ (respectively unstable solutions $\pm B_u$) displayed in figure 4. When f is increased further, a saddle-node bifurcation occurs, i.e. the stable and unstable solutions collide by pairs and disappear. This generates a limit cycle that connects the collision point with its opposite. This result can be understood as follows: the solution $B = 0$ is unstable with respect to the two different fixed points, and their opposite. It is an unstable point, whereas one of the two bifurcating solutions is a stable point, a node, and the other is a saddle. If the saddle and the node collide, say at B_c, what happens to initial conditions located close to these points? They cannot be attracted by $B = 0$ which is unstable and they cannot reach other fixed points since they just disappeared. Therefore the trajectories describe a cycle. The associated orbit contains $B = 0$ since, for a planar problem, in any orbit, there is a fixed point. Suppose that the orbit created from B_c is different from the one created by $-B_c$. These orbits being images by the transformation $\mathbf{B} \to -\mathbf{B}$, they must intersect at some point. Of course, this is not possible for a planar system because it would violate the uniqueness of the solutions. Therefore, there is only one cycle that connects points close to B_c and $-B_c$.

This provides an elementary mechanism for field reversals in the vicinity of a saddle-node bifurcation. First, in the absence of fluctuations, the limit cycle generated at the saddle-node bifurcation connects $\pm B_c$. This corresponds to

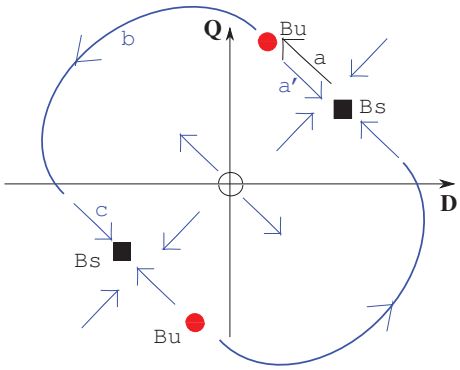

Fig. 4. A generic saddle-node bifurcation in a system with the $\mathbf{B} \to -\mathbf{B}$ invariance: below threshold, fluctuations can drive the system against its deterministic dynamics (phase a). If the effect of fluctuations is large enough, this generates a reversal (phases b and c). Otherwise, an excursion occurs (phase a').

periodic reversals. Slightly above the bifurcation threshold, the system spends most of the time close to the two states of opposite polarity $\pm B_c$. Second, in the presence of fluctuations, random reversals can be obtained slightly below the saddle-node bifurcation. B_u being very close to B_s, even a fluctuation of small intensity can drive the system to B_u from which it can be attracted by $-B_s$, thus generating a reversal.

The effect of turbulent fluctuations on the dynamics of the two magnetic modes governed by (1) can be easily modeled by adding some noisy component to the coefficients [18]. Random reversals are displayed in figure 5 (left). The system spends most of the time close to the stable fixed points $\pm B_s$. We observe in figure 5 (right) that a reversal consists of two phases. In the first phase, the system evolves from the stable point B_s to the unstable point B_u (in the phase space sketched in figure 4). The deterministic part of the dynamics acts against this evolution and the fluctuations are the motor of the dynamics. That phase is thus slow. In the second phase, the system evolves from B_u to $-B_s$, the deterministic part of the dynamics drives the system and this phase is faster.

The behaviour of the system close to B_s depends on the local flow. Close to the saddle-node bifurcation, the position of B_s and B_u defines the slow direction of the dynamics. If a component of B_u is smaller than the corresponding one of B_s, that component displays an overshoot at the end of a reversal. In the opposite case, that component will increase at the beginning of a reversal. For instance, in the phase space sketched in figure 4, the component D decreases at the end of a reversal and the signal displays an overshoot. The component Q increases just before a reversal.

For some fluctuations, the second phase does not connect B_u to $-B_s$ but to B_s. It is an aborted reversal or an excursion in the context of the Earth

dynamo. Note that during the initial phase, a reversal and an excursion are identical. In the second phase, the approaches to the stationary phase differ because the trajectory that links B_u and B_s is different form the trajectory that links B_u and $-B_s$. In particular, if the reversals display an overshoot this will not be the case of the excursion (see figure 5 (right) and the sketch of the cycle in figure 4).

Other regimes observed in the VKS experiment such as symmetric or asymmetric bursts [10] have been also described in the vicinity of more complex bifurcations of equation (1) [18].

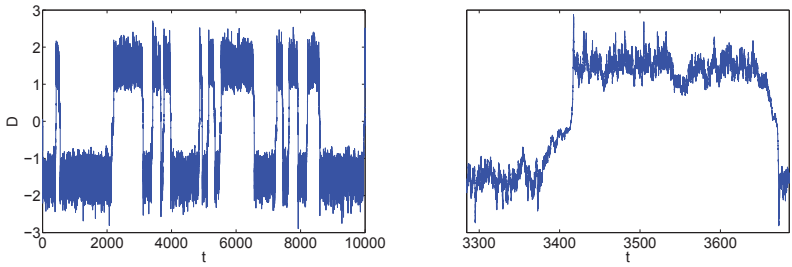

Fig. 5. Reversals of the magnetic field modeled by (1).

5 A simple model for Earth's magnetic field reversals

The above model of reversals of magnetic field in the vicinity of a saddle-node bifurcation in a system with the invariance $\mathbf{B} \to -\mathbf{B}$ explains many intriguing features of the reversals of Earth magnetic field [19]. The most significant output is that the mechanism predicts specific characteristics of the field obtained from paleomagnetic records [20], in particular their asymmetry: the Earth's dipole decays on a slower time scale than it recovers after a reversal. In addition, it displays an overshoot that immediately follows the reversals. Other characteristic features such as excursions as well as the existence of superchrons are understood in the same framework.

Although the symmetries of the flow in the Earth's core strongly differ from the ones of the VKS experiment, dipolar and quadrupolar modes can be defined with respect to equatorial symmetry such that model (1) can be transposed for Earth's magnetic field. From an analysis of paleomagnetic data, it has been proposed that reversals involve an interaction between dipolar and quadrupolar modes [21]. We thus obtain an interesting prediction about the liquid core in that case: if reversals involve a coupling of the Earth's dipole with a quadrupolar mode, then this requires that the flow in the core has broken mirror symmetry. In contrast, another scenario has been proposed in

which the Earth's dipole is coupled to an octupole, i.e., another mode with a dipolar symmetry. This does not require additional constraint on the flow in the core in the framework of our model. In any case, the existence of two coupled modes allows the system to evolve along a path that avoids $\mathbf{B} = \mathbf{0}$. In physical space, this means that the total magnetic field does not vanish during a reversal but that its spatial structure changes.

Finally, we note that reversals are also observed in purely hydrodynamic systems, in which a large scale flow driven by a turbulent background in thermal convection or in periodically driven flows, randomly reverses its direction [22]. A similar type of models can be used to understand the large scale dynamics that result from these bifurcations from turbulent flows.

References

1. Ya. B. Zeldovich, A. A. Ruzmaikin and D. D. Sokoloff, Magnetic fields in astrophysics, Gordon and Breach, New York 1983.
2. F. Pétrélis and S. Fauve, Eur. Phys. J. B **22**, 273-276 (2001).
3. S. Fauve and F. Pétrélis, C. R. Physique **8**, 87-92 (2007).
4. R. Stieglitz and U. Müller Phys. Fluids, **13**, 561 (2001); A. Gailitis et al., Phys. Rev. Lett. **86**, 3024 (2001).
5. S. Douady, Y. Couder and M. E. Brachet, Phys. Rev. Lett. **67**, 983-986 (1991)
6. S. Fauve, C. Laroche and B. Castaing, J. Physique II **3**, 271-278 (1993).
7. H. K. Moffatt, Magnetic field generation in electrically conducting fluids, Cambridge University Press, Cambridge 1978.
8. R. Monchaux et al., Phys. Rev. Lett. **98**, 044502 (2007).
9. M. Berhanu et al., Europhys. Lett. **77**, 59001 (2007).
10. F. Ravelet et al., Phys. Rev. Lett. **101**, 074502 (2008).
11. R. Monchaux et al., Phys. Fluids **21**, 035108 (2009).
12. L. Marié et al., Eur. Phys. J. B **33**, 469-485 (2003); M. Bourgoin et al., Phys. Fluids **16**, 2529-2547 (2004); F. Ravelet et al., Phys. Fluids **17**, 117104 (2005); F. Stefani et al., Eur. J. Mech. B **25** 894 (2006).
13. F. Pétrélis, N. Mordant and S. Fauve, G. A. F. D., **101**, 289-323 (2007).
14. R. Laguerre et al., Phys. Rev. Lett. **101**, 104501 (2008); **101**, 219902 (2008).
15. C. Gissinger, in preparation (2009).
16. C.Gissinger, E. Dormy and S. Fauve, Phys. Rev. Lett. **101**, 144502 (2008).
17. C. Gissinger et al., Europhys. Lett. **82**, 29001 (2008).
18. F. Pétrélis and S. Fauve, J. Phys.: Condens. Matter **20**, 494203 (2008).
19. F. Pétrélis et al., Phys. Rev. Lett. **102**, 144503 (2009).
20. J.-P. Valet, L. Meynadier and Y. Guyodo, Nature **435**, 802 (2005).
21. P. L. McFadden et al., J. Geophys. Research **96**, 3923 (1991).
22. R. Krishnamurti and L. N. Howard, Proc. Natl. Acad. Sci. **78**, 1981 (1981); J. Sommeria, J. Fluid Mech. **170**, 139 (1986); B. Liu and J. Zhang, Phys. Rev. Letters, **100**, 244501 (2008) and references therein.